


Confirmation of stimulated Hawking radiation, but not of black hole lasing

Jeff Steinhauer

Department of Physics, Technion-Israel Institute of Technology, Technion City, Haifa 32000, Israel

 (Received 14 October 2021; revised 18 August 2022; accepted 5 October 2022; published 29 November 2022)

Stimulated Hawking radiation in an analog black hole in a Bose-Einstein condensate was reported in 2014, and it was claimed that the stimulation was of the black hole lasing variety. The study was based on the observation of rapidly growing negative-energy waves. We find that the correlations between the Hawking and partner particles are directly observable in the experimental plots, which confirms the stimulated Hawking radiation. We further verify this result with new measurements. Also, the observed Hawking/partner correlations provide a sensitive, background-free probe of the underlying mechanism of the stimulation. The experiment inspired the prediction of the Bogoliubov-Cherenkov-Landau (BCL) mechanism of stimulated Hawking radiation. Through a numerical simulation in which the BCL mechanism is suppressed, we find that the partner particles have an infrared cutoff due to the finite distance between the outer and inner horizons, which limits the rate of black hole lasing. We compute this cutoff for the experiment, and the resulting Bogoliubov coefficient, and black hole lasing rate. This analysis shows that the growth rate of black hole lasing is too slow to explain the observations. It is likely that the observed stimulation was due to the BCL mechanism. Furthermore, zero frequency lasing modes play no role in our numerical simulation.

DOI: [10.1103/PhysRevD.106.102007](https://doi.org/10.1103/PhysRevD.106.102007)

Stephen Hawking predicted that a black hole should spontaneously radiate a thermal spectrum [1,2]. It was not clear whether the prediction was valid in light of quantum gravity effects, such as trans-Planckian modes and back-reaction [3]. Bill Unruh suggested that these issues could be studied in a laboratory experiment [3]. This suggestion inspired a wide range of studies involving analog black holes, including stimulated Hawking radiation [4–12].

Within analog black holes in Bose-Einstein condensates [13–15], superluminal (actually supersonic) particles can resist the pull of the analog gravity, and travel outward. When these particles strike the horizon, they stimulate Hawking radiation [4], pairs of Hawking and partner particles [1,2]. In this way, the quantity of Hawking radiation exceeds the spontaneous emission. This process was first suggested in the context of black hole lasing, in which the partner particles are reflected from an inner horizon deep inside the analog black hole, and become the superluminal particles, which then stimulate additional Hawking/partner pairs [4–12,16]. This stimulated Hawking radiation was studied in an experiment in a Bose-Einstein condensate of ^{87}Rb atoms, in which the partner and superluminal particles were observed, and it was asserted that black hole lasing was the source of the superluminal particles [17]. However, this type of measurement is subject to a large, growing background, and it is difficult to isolate the Hawking radiation signal [18].

The experiment [17] inspired several theoretical studies [18–22], some with explanations other than black hole

lasing, for the observed partner and superluminal particles. One suggested that superluminal particles can be created at the inner horizon, rather than evolving from the partners as in black hole lasing [20]. This is the Bogoliubov-Cherenkov-Landau (BCL) mechanism of stimulated Hawking radiation. One of the explanations did not involve Hawking radiation at all, although it relied on reflection from a steep harmonic potential not present in the experiment [22].

Stimulated Hawking radiation was reported in a variety of other analog black and white holes [23–26], but the studies involved neither black hole lasing nor the BCL mechanism.

A later experiment with parameters different from those of Ref. [17] showed that the stimulated Hawking/partner pairs can be observed directly, rather than studying the partners and superluminal particles [27]. In light of this, we look back to the old experiment [17], and find that the Hawking/partner pairs are observable there also. This confirms the claimed observation of stimulated Hawking radiation. It also gives us a background-free observation tool for studying the Hawking radiation. We would like to determine whether black hole lasing is involved, or whether the BCL mechanism dominates instead, as in Ref. [27].

Before examining the experimental data, we will study black hole lasing in a numerical simulation, with the goal of extracting insights which are relevant for the experiments. In principle, we could compute the black hole lasing modes from the precise form of the background metric in the

simulation, and thus determine the growth rate of the lasing. However, such an approach is not applicable to experiments where the precise form is not known, so we will need to find a method of predicting the growth rate given a few general parameters of the simulation. We will use the method to determine whether the stimulated Hawking radiation in the experiment could be explained by black hole lasing.

The analog black hole consists of a Bose-Einstein condensate flowing in the positive x -direction. In the region $x < 0$ the flow velocity v_{out} is less than the speed of sound c_{out} . On the other hand, the flow is supersonic for $0 < x < L$ ($v_{\text{in}} > c_{\text{in}}$), which creates a trapping region for sound quasiparticles, in analogy with the inside of a black hole, as indicated in Fig. 1(a). The points $x = 0$ and $x = L$ correspond to the outer horizon BH and the inner horizon IH, respectively. The acceleration at $x = 0$ is achieved by an applied step potential (not shown). The potential also has an upward slope for larger x which causes the flow to slow down and become subsonic for $x > L$.

Spontaneous Hawking radiation is a thermal distribution of pairs of positive energy Hawking particles H, and negative energy partner particles P, emitted by the outer horizon. A small quantity of partner/C pairs are also produced, where the positive energy particles C are directed

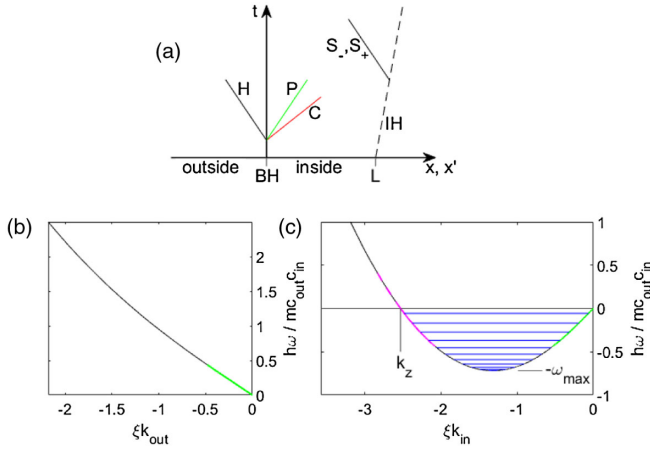


FIG. 1. Modes relevant for black hole lasing. (a) Spacetime diagram of the analog black hole. The outer and inner horizons are indicated by BH and IH, respectively. H, P, and C indicate the Hawking, partner, and comoving particles, respectively. S_- and S_+ indicate negative and positive energy supersonic particles. L indicates the length of the supersonic region. (b) The dispersion relation outside the analog black hole. The green region indicates Hawking modes H with energies less than the Hawking temperature. (c) The dispersion relation inside the analog black hole. The green region indicates partner modes P corresponding to the green region of (b). The dashed magenta region indicates S_+ particles of WHR with energies less than the Hawking-like temperature of the inner horizon. The solid magenta region are the corresponding S_- particles. ω_{max} is the ultraviolet cutoff frequency for Hawking radiation and lasing. The blue lines indicate the discrete lasing modes. k_z is the zero frequency mode.

inward in the free-falling frame (comoving with the flowing condensate). The P and C particles form a tilted sound cone inside the analog black hole. The dispersion of the Hawking particles is indicated in green in Fig. 1(b), where the maximum frequency is given by the Hawking temperature T_{H} , which is proportional to the analog surface gravity. The green curve in Fig. 1(c) indicates the dispersion of the corresponding partner particles.

Due to the superluminal dispersion relation of the Bose-Einstein condensate, the inner horizon can also spontaneously emit a thermal distribution of pairs of positive and negative energy quasiparticles referred to as “white hole radiation” (WHR), labeled S_+ and S_- in Fig. 1(a) [28]. The S_+ and S_- dispersion relations are indicated by the dashed and solid magenta curves in Fig. 1(c), where the maximum frequency is given by the Hawking-like temperature T_{I} of the inner horizon. The S_+ and S_- modes have negative group velocity, so they travel outward from the inner horizon toward the outer horizon. These particles are analogous to hypothetical superluminal trans-Planckian particles.

There are important similarities and differences between Hawking radiation and WHR. They are both a thermal, stationary population of pairs. Furthermore, in both cases, the population N_k diverges like $1/\omega$ in the 1-dimensional system. However, for Hawking radiation, k goes to zero as ω goes to zero, whereas for WHR, k remains finite as ω goes to zero, as seen in Fig. 1(c). The density amplitude of a quasiparticle is proportional to $\sqrt{N_k S_0(k)}$ [29], where $S_0(k)$ is the zero-temperature static structure factor, which is proportional to k for small k . Thus, in the Hawking radiation case, the density modulation remains finite for small ω , whereas for WHR, $S_0(k)$ remains finite, resulting in a diverging density modulation. However, the divergence occurs on a diverging timescale since ω vanishes. Thus, the density signal of the WHR continually grows in time, as seen in Ref. [28].

In black hole lasing, S_- waves impinge on the outer horizon, and stimulate additional Hawking/partner pairs. The stimulated partners reflect from the inner horizon as additional S_- waves. The reflection can involve significant amplification, depending on T_{I} . Regardless, the resulting S_- waves travel outward and stimulate yet more partners. The process repeats with a period τ_{RT} , which is the round-trip propagation time between the horizons. The stimulated Hawking radiation thus grows exponentially.

For each S_- quasiparticle which impinges on the outer horizon, $|\beta_{\text{H}}|^2$ Hawking/partner pairs are produced, where the Bogoliubov coefficient introduced by Hawking [1] is given by

$$|\beta_{\text{H}}|^2 = 1/(e^{\hbar\omega/k_{\text{B}}T_{\text{H}}} - 1) \quad (1)$$

where ω is the frequency of the S_- quasiparticle. The number of particles thus increases by a factor $|\beta_{\text{H}}|^2 + 1$ every τ_{RT} . There is a similar factor $|\beta_{\text{I}}|^2 + 1$ as a result of

the amplification at the inner horizon. The exponential growth rate for black hole lasing is thus

$$\tau_L = \frac{\tau_{RT}}{\ln[(|\beta_H|^2 + 1)(|\beta_I|^2 + 1)]} \quad (2)$$

Black hole lasing can also be understood as a finite set of discrete growing modes with complex frequency, as indicated by the blue lines in Fig. 1(c) [7]. The spacing between the modes is determined by the length L of the cavity via the condition $\Delta kL = 2\pi N$, where N is an integer, and Δk is the length of the blue line [8]. The lowest mode is set by the minimum frequency $-\omega_{\max}$. A similar situation exists for usual light lasers; the modes are discrete, but much intuition can be gained by imagining photons traveling back and forth between the mirrors. The two views are equivalent, since we can express the wave packets in terms of the discrete modes.

The reflection of the partners at the inner horizon, and their conversion to S_- particles, differentiates black hole lasing from the BCL mechanism, in which the S_- particles are produced at the inner horizon by an instability [20]. Specifically, the inside region of the analog black hole is unstable against the production of the zero frequency mode labeled k_z in Fig. 1(c). Furthermore, in realistic analog black holes, the inner horizon retreats from the outer one, as indicated by the tilted dashed line in Fig. 1(a). This produces a Doppler shift of the k_z mode, resulting in a negative frequency S_- mode in the reference frame of the outer horizon.

In the numerical simulation, we combine the outer horizon of Ref. [30] with the inner horizon of Ref. [28], and employ the Truncated Wigner method. The method of achieving the analog black hole is different from the experiment, but it is useful since it is a stationary configuration which suppresses the BCL emission from the inner horizon [28]. The simulation begins with a uniform condensate flowing with constant velocity. The speed of sound is rapidly decreased in a finite segment of the x, x' axis by decreasing the interaction between the atoms, which creates the supersonic region between the horizons. At the same time, a potential is applied between the horizons to maintain stationarity.

Figure 2 shows the normally ordered density-density correlation function from the simulation, which is defined as

$$G^{(2)}(x, x') = \sqrt{n_{\text{out}} n_{\text{in}} \xi} \left[\frac{\langle \delta n(x) \delta n(x') \rangle}{\langle n(x) \rangle \langle n(x') \rangle} - \frac{\delta(x - x')}{\langle n(x) \rangle} \right] \quad (3)$$

where $n(x)$ is the one-dimensional density, $\delta n(x)$ is its fluctuation, and n_{out} and n_{in} are the background densities. The healing length is given by $\xi = \sqrt{\xi_{\text{out}} \xi_{\text{in}}}$, where $\xi_i = \hbar/mc_i$, and m is the atomic mass. The position is indicated in units of ξ , and time is in units of $\hbar/mc_{\text{out}}c_{\text{in}}$.

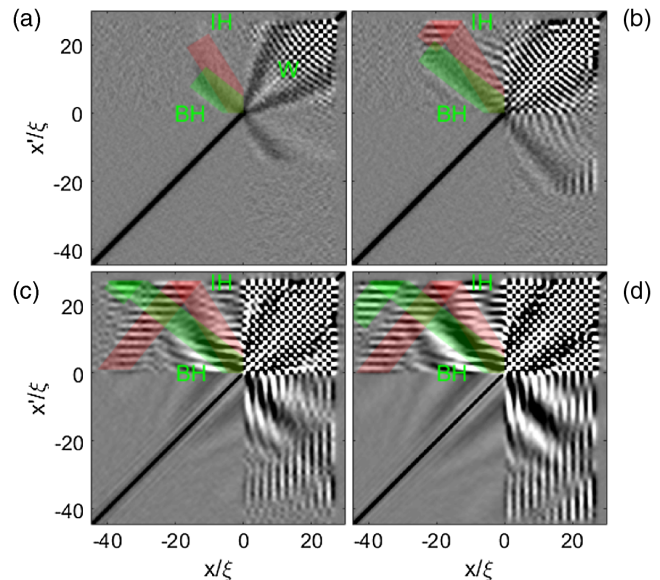


FIG. 2. Numerical simulation of black hole lasing. The density-density correlation functions at 14, 24, 40, and 46 time units are shown. (a) The green line indicates the spontaneous Hawking/partner correlations emitted from the outer horizon BH. The red line indicates the Hawking/C correlations. The checkerboard pattern at W is the white hole radiation spontaneously emitted by the inner horizon IH. (b) The Hawking/partner correlations (green line) are approaching IH. (c) The Hawking/partner correlations (green line) reflect from IH and become Hawking/S correlations with a short wavelength in the vertical direction. (d) The lasing mode has grown significantly.

The upper left quadrant of the panels of Fig. 2 shows the correlations between inside and outside the analog black hole, since $x' > 0$ is inside, and $x < 0$ is outside. Soon after the creation of the horizons, correlations between the spontaneous Hawking/partner pairs (the Hawking radiation) are seen in Fig. 2(a) as a gray band [30,31], which is highlighted with a green line. At some point in time, the partners strike the inner horizon of the analog black hole (IH in Figs. 1(a) and 2), which initiates the growth of the black hole lasing mode, as shown in the Appendix. The partners are reflected from the inner horizon in the form of supersonic S particles, as seen in Fig. 2(c), where the green Hawking/partner correlation band reflects from IH in the form of Hawking/ S correlations. The latter correlations have a short wavelength in the vertical direction, since the S mode has large wave number. By the time of Fig. 2(d), the Hawking/partner band has become much stronger than the spontaneous band seen in Fig. 2(a). This stimulated Hawking radiation is black hole lasing.

In Fig. 2(d), the Hawking/partner band exhibits an oscillatory profile, which rules out the possibility that the dominant lasing mode is a zero frequency lasing mode, which would not oscillate [9]. These modes have a slightly shorter lasing time than the finite frequency modes.

As shown in the appendix, the lasing mode starts to grow precisely when the partner quasiparticles impinge on the

inner horizon. It is thus reasonable to assume that the partners which trigger the lasing mode have the same frequency as the real part of the frequency of the lasing mode. Furthermore, the partners should have an infrared cutoff due to the finite length of the supersonic region. Therefore, the lasing mode itself should have the same cutoff. There may be other lasing modes with lower frequency, but they would not be stimulated by the partners. This infrared cutoff is in agreement with the lower right quadrant of Fig. 2(d), in which the horizontal wavelength of the lasing mode is approximately equal to the length of the supersonic region. This is verified quantitatively in the appendix.

We are now ready to write a strategy for determining the growth rate of the lasing. It assumes knowledge of the dispersion relations of the various modes. (1) Estimate the frequency of the lasing mode as being equal to the infrared cutoff, which is determined from the length of the supersonic region. (2) Determine the Hawking temperature from the observed spontaneous Hawking radiation, via our Fourier transform technique [32]. (3) Based on the physical system, estimate the relationship between $|\beta_I|^2$ and $|\beta_H|^2$ in Eq. (2). For example, $|\beta_I|^2 \approx |\beta_H|^2$ or $|\beta_I|^2 \ll |\beta_H|^2$. (4) Evaluate Eqs. (1) and (2) based on these considerations.

Using this strategy, the predicted lasing times are longer than the simulated lasing time by 30%–40%. One possible reason for this discrepancy is the symmetric outer and inner horizons. This is predicted to cause interference, which gives shorter lasing times for certain cavity lengths, and infinite lasing times for others [8]. The experiment does not have symmetric horizons, so the estimate there should be closer to the actual value. However, even the correct order of magnitude is sufficient for our purposes.

Before applying the strategy to the experiment, we will look for stimulated Hawking radiation in the experiment. Figure 3 shows a more realistic numerical simulation of the experiment, from Ref. [27]. The Hawking/partner correlations due to the stimulated Hawking radiation are visible as a gray band in the direction of the green line. This strong gray band was first discovered in the experimental plots of Ref. [27]. We can look for this band in the data from Ref. [17], as seen in Fig. 4. The band is clear in columns 2–4 of the first two rows, in the direction of the green line. It is even more apparent in the profile of the band shown in the third row (black curve and points), which has a negative peak in all columns. This confirms the observation of stimulated Hawking radiation in Ref. [17].

We have the opportunity to verify the stimulated Hawking radiation of Fig. 4 in a greatly improved experimental apparatus. Figure 5 shows new data gathered 5 years later, using the experimental apparatus of Ref. [27]. The experimental parameters are the same as in Ref. [27], with the exception of the step height, which is decreased by a factor of approximately 0.6 in order to give similar

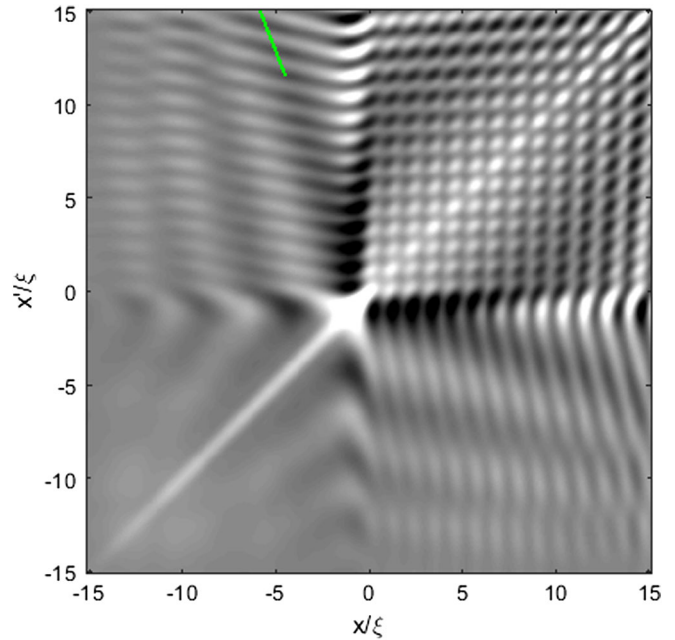


FIG. 3. Numerical simulation of the experiment from Ref. [27]. The density-density correlation function is shown. The green line is a guide to the eye.

density profiles (row 4) to Fig. 4. One indeed sees a clear Hawking/partner correlation band in all columns of Fig. 5.

With the smaller step height of Fig. 5, the correlation band is less pronounced than in Ref. [27]. This trend is also seen in Fig. 4, in which the correlation band becomes narrower and clearer from left to right. This is because the S_- waves grow faster for a smaller potential step. At some point, the amplitude is large enough that nonlinear or backreaction effects modify the correlation function. Regardless of the precise profile of the correlation band, the depth of the band is more than an order of magnitude deeper than expected for spontaneous Hawking radiation, which demonstrates that the Hawking radiation is stimulated.

Figure 6 shows the growth of the correlation band from Fig. 4. The exponential fits give time constants of 62, 17, and 27 ms for the small, medium, and large potential steps, respectively. We can compare these time constants to the expectation for black hole lasing, computed by the method found above for the simulation. We assume a Hawking temperature of $k_B T_H = 0.35$ nK as in Ref. [33]. This is an optimistic estimate, since the step potential was sharper in Ref. [33] than in Ref. [17]. From the length of the lasing region and the propagation speed of the partners, the infrared cutoff is 29, 31, and 23 Hz for the small, medium, and large potential steps, respectively. To find the minimum possible lasing time, we can assume that $|\beta_I|^2 = |\beta_H|^2$, although $|\beta_I|^2$ is likely smaller since the inner horizon is gradual, whereas the outer horizon is imposed by a steep potential step. Combining this with $\tau_{RT} = 57, 55,$ and 78 ms from Ref. [17], this gives minimum lasing times of

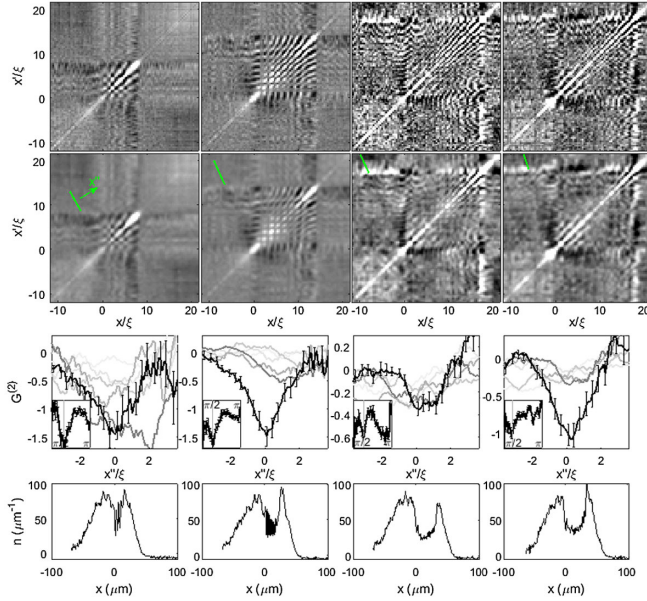


FIG. 4. Hawking/partner correlations in the experiment of Ref. [17]. The first through third columns show small, medium, and large step heights, respectively. The fourth column shows the large step 20 ms later. The first row shows the raw correlation function. The second row is smoothed (convoluted with a Gaussian) to improve the visibility of the Hawking/partner correlation band. The green line indicates the angle of the Hawking/partner correlation band, which is determined in the inset of the third row. The third row (black curve) shows the profile of the correlation band in the x'' direction, which is perpendicular to the band. The profile is computed by integrating the second row along parallel segments at the angle found in the inset. The gray curves show earlier times separated by 20 ms, where the darker the gray the later the time. The inset shows the angular profile of the second row. The gray line indicates the minimum of the correlation band, which gives the angle of the band. The fourth row shows the ensemble-averaged density profile.

1.6, 2.0, and 0.8 s. These values are almost 2 orders of magnitude longer than the experimental values given above. Thus, one concludes that the stimulated Hawking radiation is not black hole lasing. It is likely that the stimulation is due to the BCL mechanism, as in Ref. [27].

There is an additional effect which can further lengthen the lasing time. Simulations suggest that the inner horizon should move away from the outer horizon with a velocity v_{IH} , as illustrated in Fig. 1(a) [20]. In black hole lasing, the partners reflect from this moving horizon, which causes a Doppler shift $k_0 v_{\text{IH}}$ in the frequency of the S particles, where k_0 is their large wave number. This increase in frequency will decrease the rate of black hole lasing by Eqs. (1) and (2). We can evaluate v_{IH} in the experimental data of Ref. [17]. Figure 7 shows the position of the inner horizon as a function of time. The data shows a slight positive slope. The linear fits give $v_{\text{IH}} = 14(8)$, $18(17)$, and $18(26) \mu\text{m s}^{-1}$ for the small, medium, and large steps, respectively. The wavelength of the density oscillations in

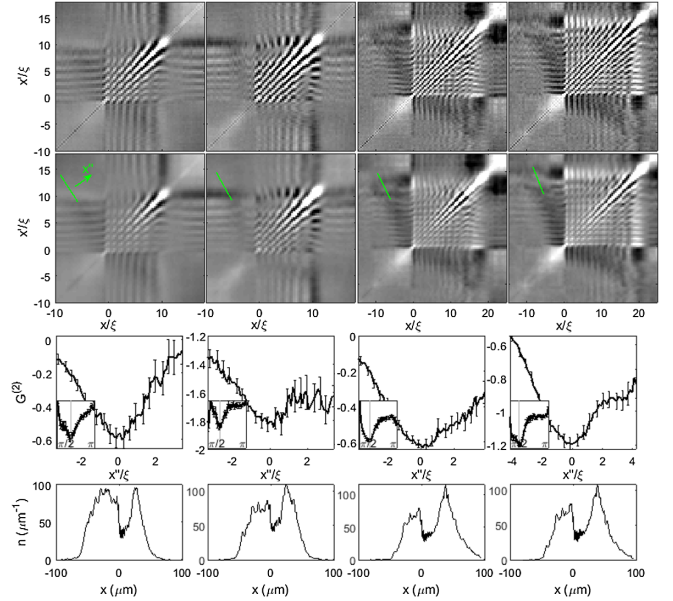


FIG. 5. Stimulated Hawking radiation in the new experiment. The description of the rows is the same as in Fig. 4. From left to right, the 4 columns show relative step heights of 0.59, 0.59, 0.60, and 0.65, respectively. The second column shows 66.5 ms later than the first column.

the fourth row of Fig. 4 yield $k_0 = 1.7, 2.3, \text{ and } 2.8 \mu\text{m}^{-1}$. Thus, the Doppler shifts are $k_0 v_{\text{IH}}/2\pi = 4(2)$, $7(6)$, and $8(12)$ Hz. These values provide a lower bound on $\omega/2\pi$, since they neglect the contribution of the Hawking temperature. Taking $\omega/2\pi$ to be this lower bound gives lasing times of 60, 110, and 180 ms. We see that this effect is less significant than the infrared cutoff, but it still limits the lasing time to a value longer than the observed growth time, in most cases.

Previous numerical simulations [20,21] also found a lack of black hole lasing in Ref. [17]. However, one of these simulations [20] had a v_{IH} which was 5 times faster than in [17], which would greatly increase τ_{L} . The simulation in Ref. [21] was likely improved in this respect, and it reached the same findings.

The BCL mechanism is the alternative to black hole lasing. Its growth rate is determined by the emission

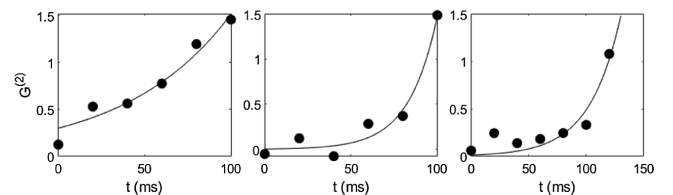


FIG. 6. Growth of the experimental correlations. The growth of the minimum in the third row of Fig. 4 is shown. The first and second columns correspond to the first and second columns of Fig. 4, respectively. The third column corresponds to the third and fourth columns of Fig. 4.

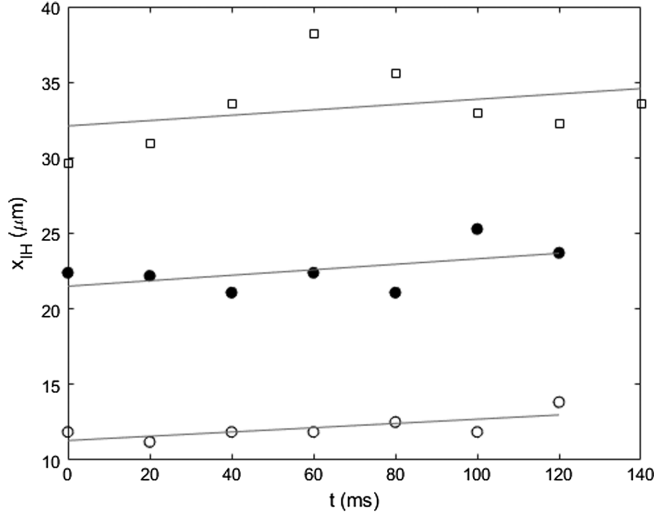


FIG. 7. Motion of the inner horizon in Ref. [17]. The position of the inner horizon is shown for the small step (open circles), medium step (filled circles), and large step (squares). The lines are linear fits.

rate of S_- particles from the inner horizon. This rate increases as the square of the background density in the supersonic region [20]. The small potential steps considered in this work result in an increased background density, so the BCL growth should be even faster than in Ref. [27].

In conclusion, stimulated Hawking radiation is confirmed in the 2014 experiment, by direct observation of the Hawking/partner pair correlations. The result is further supported by new measurements. The observed pairs provide a sensitive test of the mechanism of stimulated Hawking radiation. Through a numerical simulation of black hole lasing, we see that the lasing is triggered by the partner particles. These particles have an infrared cutoff due to the finite distance between the outer and inner horizons. Thus, the lasing mode likely has the same cutoff. Computing this cutoff for the experiment, and the resulting Bogoliubov coefficient, we find that the rate of black hole lasing would be too small to explain the pair production in the experiment. Even if the infrared cutoff is not relevant for the experiment, the motion of the inner horizon would limit the lasing rate to a value lower than the experimentally observed rate, in most cases. These considerations suggest that the BCL mechanism dominates, as found in a different experiment.

ACKNOWLEDGMENTS

I thank J. R. M. de Nova for performing the numerical simulations. I thank F. Michel for helpful comments. This work was supported by the Israel Science Foundation.

APPENDIX: DETERMINING THE LASING TIME CONSTANT

In this appendix, we will evaluate the expected black hole lasing time constant for the simulation via Eqs. (1)

and (2). The actual simulated lasing time constant will also be extracted.

We can quantitatively study the simulated correlation patterns by means of our Fourier transform technique [32]. The two-dimensional Fourier transform of the upper left quadrant of the correlation function gives us the correlations between the Hawking and partner modes, by the relation [32]

$$S_0 \langle \hat{b}_H \hat{b}_P \rangle = \frac{\xi}{\sqrt{L_{\text{out}} L_{\text{in}}}} \int dx dx' e^{ik_H x} e^{ik_P x'} G^{(2)}(x, x') \quad (\text{A1})$$

where \hat{b}_H and \hat{b}_P are annihilation operators for Hawking and partner particles, S_0 is the geometric mean of $S_0(k)$ for the Hawking and partner particles, and $L_{\text{out(in)}}$ is the effective length of the region outside (inside) the analog black hole. The ratio of L_{out} and L_{in} is given by the ratio of the wave propagation speeds

$$\frac{L_{\text{out}}}{L_{\text{in}}} = \frac{c_{\text{out}} - v_{\text{out}}}{v_{\text{in}} - c_{\text{in}}} \quad (\text{A2})$$

In other words, the Hawking/partner correlation band in the correlation function should cross opposite corners of a rectangle of dimension $L_{\text{out}} \times L_{\text{in}}$, as illustrated by the green rectangle in Fig. 8.

Figure 9(a) shows the correlation pattern at an early time before the partners have struck the inner horizon. Thus, the Hawking radiation and WHR are of the spontaneous type. The Fourier transform within the green rectangle in the upper left quadrant gives us the correlations between the Hawking and partner quasiparticles as seen in Fig. 9(b), where the vertical (horizontal) axis is inside (outside). The green curve indicates the k -values for Hawking/partner

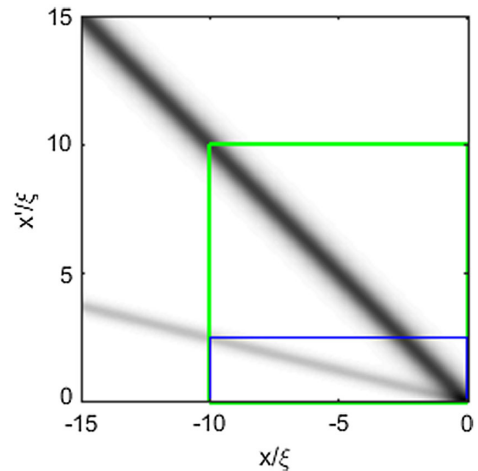


FIG. 8. The relevant regions for the Fourier transform. The Hawking/partner correlation band crosses the corners of the green rectangle. The vertical (horizontal) dimension of the green rectangle is L_{in} (L_{out}). The blue rectangle corresponds to a large k -value.

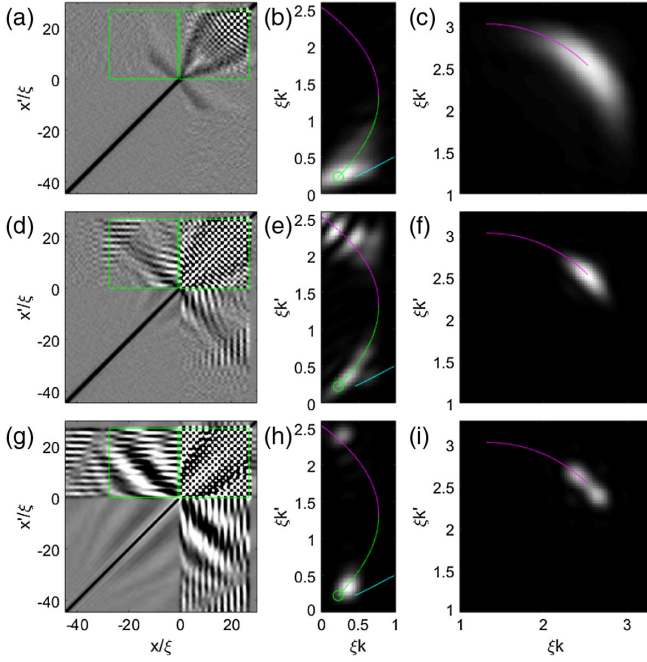


FIG. 9. Fourier transform of the simulated correlation patterns. The first column shows the density-density correlation function at times of 12, 32, and 52. The second (third) column shows the magnitude squared of the Fourier transform within the left (right) green square of the first column. In the second column, the green, cyan, and magenta curves indicate Hawking/partner pairs, Hawking/C pairs, and Hawking/ S_- pairs, respectively. The green circle is the infrared cutoff. In the third column, the magenta curve indicates the WHR correlations between the S_-/S_+ pairs.

pairs along the green curves of Figs. 1(b) and 1(c). Some correlations are also visible along the cyan curve, which are Hawking/C correlations. The upper right quadrant of Fig. 9(a) shows correlations between pairs of points, both of which are located inside the analog black hole. The Fourier transform within the green square in this quadrant gives the correlations of the S_+/S_- pairs of the spontaneous WHR, as shown in Fig. 9(c).

By the time of the third row of Fig. 9, the stimulated Hawking radiation (the black hole lasing) dominates over the spontaneous contribution, as seen through the strong Hawking/partner correlations in the upper left quadrant of Fig. 9(g). The Fourier transforms seen in Figs. 9(h) and 9(i) have become pointlike, since a single lasing mode dominates, in contrast to the spontaneous thermal spectra of Figs. 9(b) and 9(c).

We would like to compute the expected lasing time from Eq. (2). In order to do this, we will need to know $|\beta_H|^2$. By Eq. (1), this quantity is a function of T_H , which can be extracted from the simulation at early times for which the Hawking radiation is still spontaneous.

For the sake of determining T_H , the right side of Eq. (A1) can be evaluated from the spontaneous correlation pattern, while the left side can be expressed in terms of $|\beta_H|^2$. Specifically,

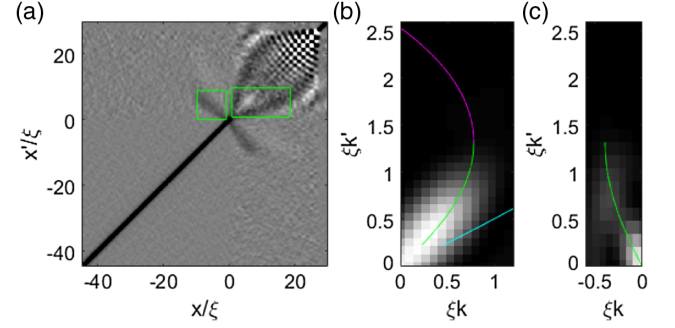


FIG. 10. Spontaneous Hawking radiation in the simulation. A time of 10 is shown. (a) The density-density correlation function. (b) The magnitude squared of the Fourier transform within the green square of (a). The green, cyan, and magenta curves indicate Hawking/partner pairs, Hawking/C pairs, and Hawking/ S_- pairs, respectively. (c) The magnitude squared of the Fourier transform within the green rectangle in (a). The green curve indicates the partner/C correlations.

$$S_0^2 = \frac{(\xi_{\text{out}} k_H)^2}{\sqrt{4(\xi_{\text{out}} k_H)^2 + (\xi_{\text{out}} k_H)^4}} \frac{(\xi_{\text{in}} k_P)^2}{\sqrt{4(\xi_{\text{in}} k_P)^2 + (\xi_{\text{in}} k_P)^4}} \quad (\text{A3})$$

and

$$|\langle \hat{b}_H \hat{b}_P \rangle|^2 = |\alpha_H|^2 |\beta_H|^2 \quad (\text{A4})$$

where $|\alpha_H|^2$ is given by [34]

$$|\alpha_H|^2 = 1 + |\beta_H|^2 + |\gamma_H|^2 \quad (\text{A5})$$

and α_H and γ_H are the Bogoliubov coefficients for the production of partner and C modes respectively, from incoming S_- particles. Figure 10 shows the correlation pattern and its Fourier transforms during the spontaneous period. The Hawking/partner correlations [the magnitude squared of the right side of Eq. (A1)] along the green curve in Fig. 10(b) are indicated by the black curve in Fig. 11, where each point is a weighted average of nearby pixels in Fig. 10(b). The gray curve in Fig. 11 shows a slightly earlier time. Low k -values are not shown since they are affected by the Hawking/C correlations along the cyan curve in Fig. 10(b). These positive correlations are also seen as a light gray region within the upper part of the green square in Fig. 10(a). These Hawking/C correlations are much stronger than those of the experiment due to the low ultraviolet cutoff ω_{max} in the simulation.

Another effect of the low ultraviolet cutoff in the simulation is that the Hawking temperature is close to the cutoff. This implies that there is a significant population of Hawking/partner pairs close to the cutoff. The partners have vanishing group velocity near the cutoff, as seen in Fig. 1(c). This must be accounted for in Eq. (A1), as explained in Ref. [34], which states that the ratio $L_{\text{out}}/L_{\text{in}}$

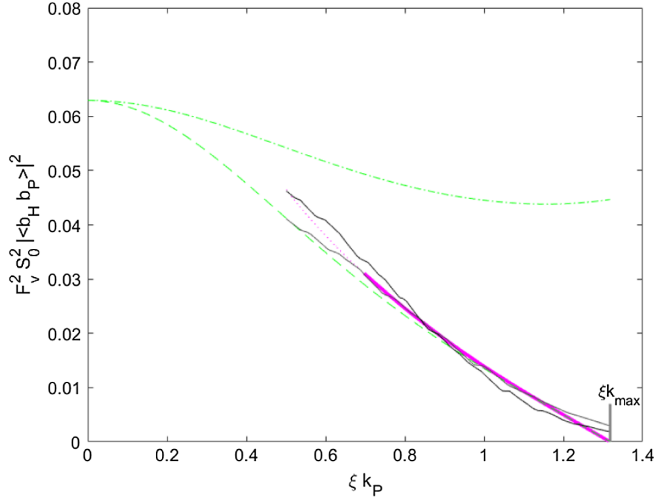


FIG. 11. The simulated correlation spectrum of spontaneous Hawking radiation. The gray and black curves correspond to times of 8 and 10, respectively. The solid region of the magenta curve is fit to the gray and black curves, by adjusting the Hawking temperature. The green curves neglect the effect of the C modes. The dash-dotted green curve neglects the effect of the varying group velocity.

should be given by the ratio of the group velocities rather than by Eq. (A2), so the Fourier transform should be computed in rectangles of various aspect ratios, depending on k . However, this prescription is impractical for experimental data, or even for simulations, because it requires evaluating the Fourier transform in a rectangle with a diverging aspect ratio. An extremely long rectangle would have extremely large area, which would introduce diverging noise in the case of experimental data. It would also require an extremely large measurement system.

We propose an alternative method to account for the $L_{\text{out}}/L_{\text{in}}$ ratio. The right side of Eq. (A1) should be independent of L_{out} and L_{in} , as long as they have the correct ratio. Thus, we understand that the area integral should increase like a length. This suggests that the integrand is a long narrow band of finite cross section, as illustrated by the light gray band in Fig. 8. For this k -value, we should compute the Fourier transform within the blue rectangle. On the other hand, in Eqs. (A1) and (A2), we use the green rectangle (the small- k rectangle) for all k . However, we can see that the Fourier transform of the light gray band is the same, regardless of whether it is computed in the blue or green rectangle, since the light gray band has approximately zero value outside the blue rectangle. Thus, there is no need to adjust the region used for the integral in Eq. (A1), for each k . One only needs to adjust the value of L_{in} in the prefactor, in order to maintain the correct $L_{\text{out}}/L_{\text{in}}$ ratio for each k . This additional prefactor would depend on knowledge of the dispersion relation, so it seems more appropriate to put this factor on the left theory side of the equation, and to leave the right side as the measurement. Equation (A1) becomes

$$F_v S_0 \langle \hat{b}_H \hat{b}_P \rangle = \frac{\xi}{\sqrt{L_{\text{out}} L_{\text{in}}}} \int dx dx' e^{ik_H x} e^{ik_P x'} G^{(2)}(x, x') \quad (\text{A6})$$

where

$$F_v \equiv \sqrt{\frac{v_g^{\text{in}} c_{\text{out}} - v_{\text{out}}}{v_g^{\text{out}} v_{\text{in}} - c_{\text{in}}}} \quad (\text{A7})$$

where v_g^i is the group velocity in each region.

The dashed green curve of Fig. 11 indicates the magnitude squared of the left side of Eq. (A6), computed with Eqs. (A3), (A4), (A5) (without the $|\gamma_H|^2$ term for now), and (A7), where $k_B T_H$ has been adjusted to $0.45 m c_{\text{out}} c_{\text{in}}$, as discussed below. If the F_v factor is neglected, one obtains the dash-dotted green curve, which is far from the black and gray simulation curves. We thus see that the F_v factor gives a good result in the presence of the low ultraviolet cutoff. Furthermore, the factor seems reasonable as explained above. However, a precise test of the method is beyond the scope of this work. Such a test could be performed on the precisely stationary analytical correlation functions of Ref. [35].

Now we shall add the $|\gamma_H|^2$ term. This quantity is similar to $|\beta_H|^2$, but for the production of C particles rather than Hawking particles. Figure 12 shows the profiles along the green curve of Fig. 10(c) for two different times, where each point is a weighted average of nearby pixels in Fig. 10(c). Computing the ratio of these curves to the black and gray curves of Fig. 11, and accounting for the F_v factors, gives the ratio between the $|\gamma_H|^2$ and $|\beta_H|^2$ coefficients. Including $|\gamma_H|^2$ in Eq. (A5) results in the dotted magenta curve of Fig. 11.

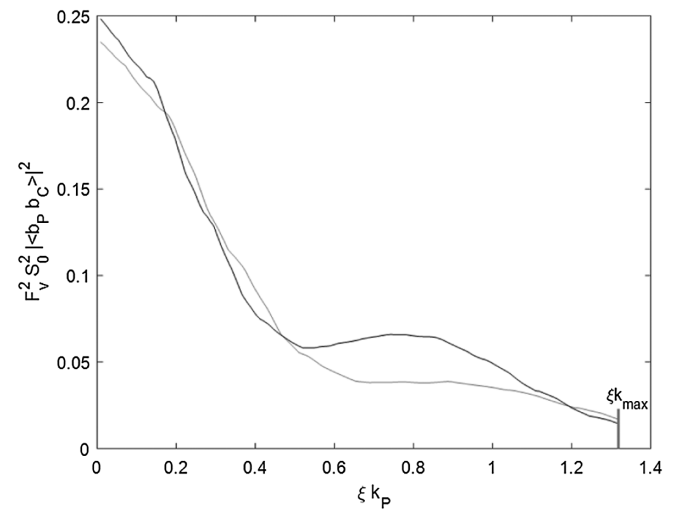


FIG. 12. The simulated correlation spectrum of the partner and C modes. The gray and black curves correspond to times of 8 and 10, respectively.

We extract the Hawking temperature from Fig. 11 by fitting the magenta curve to the black and gray curves in the region indicated by the solid magenta curve. The fit gives a Hawking temperature of $k_B T_H = 0.45 mc_{\text{out}} c_{\text{in}}$. This value is not far from the ultraviolet cutoff $0.72 mc_{\text{out}} c_{\text{in}}$; it is only smaller by a factor of 0.6. In contrast, in the experiment of Ref. [33], the Hawking temperature is smaller than the ultraviolet cutoff by a factor of 0.1, so the cutoff plays a negligible role. We can understand this difference between the simulation and the experiment by considering the flow velocity, since the cutoff is on the order of $mv_{\text{in}}^2/2$. In the experiment, $v_{\text{in}} > c_{\text{out}}$, so there is a large cutoff. In contrast, the simulation has the same flow velocity on both sides of the horizon ($v_{\text{out}} = v_{\text{in}}$). The flow outside is necessarily subsonic, so $v_{\text{in}} < c_{\text{out}}$. Thus, the simulation inherently has a low ultraviolet cutoff. For the simulation discussed here, $v_{\text{in}} = 0.6c_{\text{out}}$.

In addition to the Hawking temperature, we need the frequency of the lasing mode in order to evaluate $|\beta_H|^2$. We can see the lasing mode along the green curve in Fig. 9(h). Through the dispersion relation, we can see that the frequency of this point is $0.25 mc_{\text{out}} c_{\text{in}}/\hbar$. Equation (1) then gives $|\beta_H|^2 = 1.30$. To evaluate Eq. (2), we will need $|\beta_1|^2$. Since the outer and inner horizons are symmetric, we assume that $|\beta_1|^2 = |\beta_H|^2$. In this case, the predicted lasing time from Eq. (2) is 30 time units. We can make a similar prediction without directly using the frequency of the lasing mode, by noting that it is close to the infrared cutoff (the green circle) in Fig. 9(h). This is reasonable since the dominant lasing mode is the one with the shortest τ_L , which implies lowest frequency. As stated in the main text, we can also see that the dominant lasing mode is close to the infrared cutoff by inspecting Fig. 9(g), since the horizontal wavelength in the lower right quadrant is close to the entire length of the lasing region. The infrared cutoff frequency is given by $0.21 mc_{\text{out}} c_{\text{in}}/\hbar$. Taking this as the frequency of the lasing mode gives a predicted lasing time of 27 time units.

In order to plot the simulated growth of the lasing mode, we focus on two quantities. First, the magnitude of the Hawking/partner correlations from Fig. 10(b) are indicated by the blue curve of Fig. 13. Second, the upper point along the magenta curve in Fig. 9(h) is the

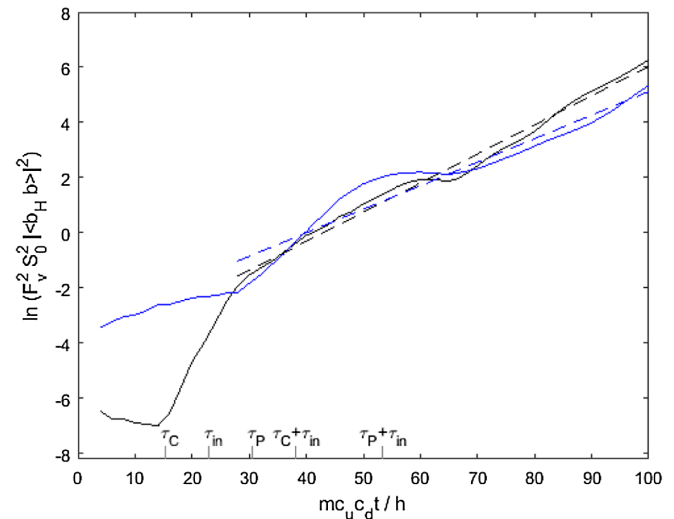


FIG. 13. The simulated growth of the lasing mode. The blue curve is the correlations between the Hawking and P modes. The black curve is the correlations between the Hawking and S_- modes. The times τ_C and τ_P are the times required for the C and P modes to travel from the outer horizon to the inner horizon. The time τ_{in} is the time for the S modes to travel from the inner horizon to the outer horizon.

Hawking/ S_- correlations of the lasing mode. Its magnitude is indicated by the black curve of Fig. 13. Since Fig. 13 shows the growth of the single lasing mode, maximum pixel values are shown. At early times, the Hawking radiation is spontaneous, and the blue curve is almost constant. The partner particles strike the inner horizon at the time τ_P , which triggers the lasing, and the blue curve starts to increase. The dashed blue line is a linear fit for times after τ_P , and its slope gives the lasing time.

The emission from the two horizons is uncorrelated for the earliest times, as reflected in the low value of the black curve of Fig. 13. The spontaneously emitted C modes are the first to traverse the distance between the horizons. They reach the inner horizon at the time τ_C , which causes correlations between the horizons, and the black curve begins to increase. It joins the blue curve when the lasing begins. The average slope of the two linear fits of Fig. 13 give a lasing time of 21 time units (the quantity plotted grows like $2\tau_L^{-1}$).

-
- [1] S. W. Hawking, Black hole explosions?, *Nature (London)* **248**, 30 (1974).
 [2] S. W. Hawking, Particle creation by black holes, *Commun. Math. Phys.* **43**, 199 (1975).
 [3] W. G. Unruh, Experimental Black-Hole Evaporation?, *Phys. Rev. Lett.* **46**, 1351 (1981).

- [4] S. Corley and T. Jacobson, Black hole lasers, *Phys. Rev. D* **59**, 124011 (1999).
 [5] P. Jain, A. S. Bradley, and C. W. Gardiner, Quantum de Laval nozzle: Stability and quantum dynamics of sonic horizons in a toroidally trapped Bose gas containing a superflow, *Phys. Rev. A* **76**, 023617 (2007).

- [6] U. Leonhardt and T. G. Philbin, Quantum analogues: From phase transitions to black holes and cosmology, *Lect. Notes Phys.* **718**, 229 (2007).
- [7] A. Coutant and R. Parentani, Black hole lasers, a mode analysis, *Phys. Rev. D* **81**, 084042 (2010).
- [8] S. Finazzi and R. Parentani, Black hole lasers in Bose-Einstein condensates, *New J. Phys.* **12**, 095015 (2010).
- [9] F. Michel and R. Parentani, Saturation of black hole lasers in Bose-Einstein condensates, *Phys. Rev. D* **88**, 125012 (2013).
- [10] J. R. M. de Nova, P. F. Palacios, I. Carusotto, and F. Sols, Long time universality of black-hole lasers, *New J. Phys.* **23**, 023040 (2021).
- [11] J. L. Gaona-Reyes and D. Bermudez, The theory of optical black hole lasers, *Ann. Phys. (Amsterdam)* **380**, 41 (2017).
- [12] J. D. Rincon-Estrada and D. Bermudez, Instabilities in an optical black-hole laser, *Ann. Phys. (Amsterdam)* **533**, 2000239 (2021).
- [13] L. J. Garay, J. R. Anglin, J. I. Cirac, and P. Zoller, Sonic Analog of Gravitational Black Holes in Bose-Einstein Condensates, *Phys. Rev. Lett.* **85**, 4643 (2000).
- [14] C. Barceló, S. Liberati, and M. Visser, Analogue gravity from Bose Einstein condensates, *Classical Quantum Gravity* **18**, 1137 (2001).
- [15] J. Macher and R. Parentani, Black-hole radiation in Bose Einstein condensates, *Phys. Rev. A* **80**, 043601 (2009).
- [16] J. R. M. de Nova, S. Finazzi, and I. Carusotto, Time-dependent study of a black-hole laser in a flowing atomic condensate, *Phys. Rev. A* **94**, 043616 (2016).
- [17] J. Steinhauer, Observation of self-amplifying Hawking radiation in an analogue black-hole laser, *Nat. Phys.* **10**, 864 (2014).
- [18] J. Steinhauer and J. R. M. de Nova, Self-amplifying Hawking radiation and its background: A numerical study, *Phys. Rev. A* **95**, 033604 (2017).
- [19] M. Tettamanti, S. L. Cacciatori, A. Parola, and I. Carusotto, Numerical study of a recent black-hole lasing experiment, *Europhys. Lett.* **114**, 60011 (2016).
- [20] Y.-H. Wang, T. Jacobson, M. Edwards, and C. W. Clark, Mechanism of stimulated Hawking radiation in a laboratory Bose-Einstein condensate, *Phys. Rev. A* **96**, 023616 (2017).
- [21] Y.-H. Wang, T. Jacobson, M. Edwards, and C. W. Clark, Induced density correlations in a sonic black hole condensate, *SciPost Phys.* **3**, 022 (2017).
- [22] M. Tettamanti, I. Carusotto, and A. Parola, On the role of interactions in trans-sonically flowing atomic condensates, *Europhys. Lett.* **133**, 20002 (2021).
- [23] S. Weinfurter, E. W. Tedford, M. C. J. Penrice, W. G. Unruh, and G. A. Lawrence, Measurement of Stimulated Hawking Emission in an Analogue System, *Phys. Rev. Lett.* **106**, 021302 (2011).
- [24] G. Rousseaux, C. Mathis, P. Maïssa, T. G. Philbin, and U. Leonhardt, Observation of negative-frequency waves in a water tank: A classical analogue to the Hawking effect?, *New J. Phys.* **10**, 053015 (2008).
- [25] L.-P. Euvé, F. Michel, R. Parentani, T. G. Philbin, and G. Rousseaux, Observation of Noise Correlated by the Hawking Effect in a Water Tank, *Phys. Rev. Lett.* **117**, 121301 (2016).
- [26] J. Drori, Y. Rosenberg, D. Bermudez, Y. Silberberg, and U. Leonhardt, Observation of Stimulated Hawking Radiation in an Optical Analogue, *Phys. Rev. Lett.* **122**, 010404 (2019).
- [27] V. I. Kolobov, K. Golubkov, J. R. M. de Nova, and J. Steinhauer, Observation of stationary spontaneous Hawking radiation and the time evolution of an analogue black hole, *Nat. Phys.* **17**, 362 (2021).
- [28] C. Mayoral, A. Recati, A. Fabbri, R. Parentani, R. Balbinot, and I. Carusotto, Acoustic white holes in flowing atomic Bose-Einstein condensates, *New J. Phys.* **13**, 025007 (2011).
- [29] I. Shammass, S. Rinott, A. Berkovitz, R. Schley, and J. Steinhauer, Phonon Dispersion Relation of an Atomic Bose-Einstein Condensate, *Phys. Rev. Lett.* **109**, 195301 (2012).
- [30] I. Carusotto, S. Fagnocchi, A. Recati, R. Balbinot, and A. Fabbri, Numerical observation of Hawking radiation from acoustic black holes in atomic Bose-Einstein condensates, *New J. Phys.* **10**, 103001 (2008).
- [31] R. Balbinot, A. Fabbri, S. Fagnocchi, A. Recati, and I. Carusotto, Nonlocal density correlations as a signature of Hawking radiation from acoustic black holes, *Phys. Rev. A* **78**, 021603(R) (2008).
- [32] J. Steinhauer, Measuring the entanglement of analogue Hawking radiation by the density-density correlation function, *Phys. Rev. D* **92**, 024043 (2015).
- [33] J. R. M. de Nova, K. Golubkov, V. I. Kolobov, and J. Steinhauer, Observation of thermal Hawking radiation and its temperature in an analogue black hole, *Nature (London)* **569**, 688 (2019).
- [34] M. Isoard and N. Pavloff, Departing from Thermality of Analogue Hawking Radiation in a Bose-Einstein Condensate, *Phys. Rev. Lett.* **124**, 060401 (2020).
- [35] P.-E. Larre, A. Recati, I. Carusotto, and N. Pavloff, Quantum fluctuations around black hole horizons in Bose-Einstein condensates, *Phys. Rev. A* **85**, 013621 (2012).